

Purely electrical detection of the Néel vector of p -wave magnets based on linear and nonlinear conductivities

Motohiko Ezawa¹

¹*Department of Applied Physics, The University of Tokyo, 7-3-1 Hongo, Tokyo 113-8656, Japan*
(Dated: October 30, 2024)

A p -wave magnet has a momentum-dependent band structure and zero-net magnetization just as in the case of an altermagnet. It will be useful for high-density and ultra-fast memory. However, it is a nontrivial problem to detect the Néel vector of a p -wave magnet because time-reversal symmetry is preserved, while this is not a problem in an altermagnet because the anomalous Hall conductivity may be present due to the breaking of time-reversal symmetry. Here, we show that it is possible to detect the in-plane component of the Néel vector of the p -wave magnet by measuring the transverse and longitudinal Drude conductivity. Remarkably, this is possible without magnetization. Furthermore, it is possible to detect the z -component by measuring nonlinear conductivity including the nonlinear Drude conductivity and quantum-metric induced nonlinear conductivity by introducing tiny magnetization along the z axis. We obtain analytic formulae for them in the first-order perturbation theory, which agree quite well with numerical results without perturbation. Our results will pave a way to spintronic memory based on p -wave magnets.

Introduction

Ferromagnets are useful for nonvolatile memories, where the up and down spins act as a bit. On the other hand, antiferromagnets are expected to act as more efficient memories owing to their zero net magnetization, where high-density and quick-switchable memories may be possible. However, it is very hard to readout the direction of the Néel vector of antiferromagnet[1–7]. Recently, altermagnets attract growing interests[8–10] because they have both merits of ferromagnets and antiferromagnets. Altermagnets have zero net magnetization and they break time-reversal symmetry. Accordingly, the Néel vector is observable by means of the anomalous Hall conductivity[11–14]. A characteristic feature of altermagnets which is absent in both ferromagnets and antiferromagnets is the momentum-dependent band structure[8–10, 15–17], which includes the d -wave, g -wave and i -wave band structures. Indeed, momentum dependent band structures have been observed by Angle-Resolved Photo-Emission Spectroscopy (ARPES)[18–22]. Furthermore, spin current is generated in d -wave altermagnets[17, 23–25].

A p -wave magnet was proposed only recently[26]. They have zero net magnetization as well. They resemble altermagnets from a point of view that they have momentum-dependent band structure with the p -wave symmetry. However, they preserve time-reversal symmetry, which leads to the zero anomalous Hall conductivity. There is so far no known method to detect the Néel vector of p -wave magnets, which makes difficult to use them for spintronics.

The linear conductivity $\sigma^{a;b}$ is defined by $j^b = \sigma^{a;b} E^a$, where E^a is an applied electric field along the a direction and j^b is the current along the b direction. They include the longitudinal Drude conductivity $\sigma^{x;x}$ and the transverse Drude conductivity $\sigma^{y;x}$. On the other hand, there are several studies on nonlinear conductivity[27–39]. Especially, the second-order nonlinear conductivity $\sigma^{ab;c}$ is defined by $j^c = \sigma^{ab;c} E^a E^b$, where E^a is an applied electric field along the a direction and j^c is the current along the c direction. Among them, the nonlinear Drude conductivity is proportional to τ , where τ is the electron relaxation time. It is an extrinsic nonlinear conductivity,

while the quantum-metric induced nonlinear conductivity is intrinsic because it is irrelevant to τ .

In this paper, we show that the in-plane component of the Néel vector of p -wave magnets is detectable by measuring the transverse and longitudinal linear Drude conductivities. Remarkably, this is possible without magnetization. In addition, the z -component of the Néel vector of p -wave magnets is detectable by measuring the nonlinear conductivity with the aid of the magnetization along the z axis. We obtain analytic formulae for linear and nonlinear conductivities based on a perturbation theory with respect to the magnitude J of the Néel vector and magnetization B , which agree quite well with numerical results without perturbation.

Model

We analyze a system where a p -wave magnet is placed on a substrate as shown in Fig.1a. The substrate breaks inversion symmetry and induces the Rashba interaction. Then, the Hamiltonian is given by

$$H = H_0 + H_\lambda + H_p. \quad (1)$$

The first term represents the kinetic energy of free fermions

$$H_0 = M(k_x, k_y) \sigma_0 \quad (2)$$

with $M(k_x, k_y) = \hbar^2 (k_x^2 + k_y^2) / (2m)$, where m is the free-fermion mass, and σ_0 is 2×2 identity matrix. The second term represents the Rashba interaction

$$H_\lambda = \lambda (-k_y \sigma_x + k_x \sigma_y), \quad (3)$$

where λ is the magnitude of the spin-orbit interaction, and σ_x and σ_y are the Pauli matrix for the spin. The third term

$$H_p(\mathbf{k}) = J(\mathbf{s} \cdot \boldsymbol{\sigma}) k_x \quad (4)$$

describes the effect of the p -wave magnet[26, 40, 41] with the direction of the Néel vector $\mathbf{s} = (\sin \Theta \cos \Phi, \sin \Theta \sin \Phi, \cos \Theta)$, where J is the magnitude of the p -wave magnet, and $J\mathbf{s}$ is the Néel vector. Then, we have $J_x = J \sin \Theta \cos \Phi$, $J_y = J \sin \Theta \sin \Phi$ and $J_z = J \cos \Theta$.

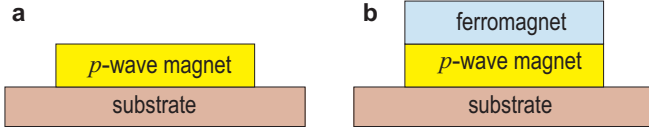


FIG. 1. Illustration of the system made of **a** p-wave-magnet-substrate structure and **b** ferromagnet-p-wave-magnet-substrate structure.

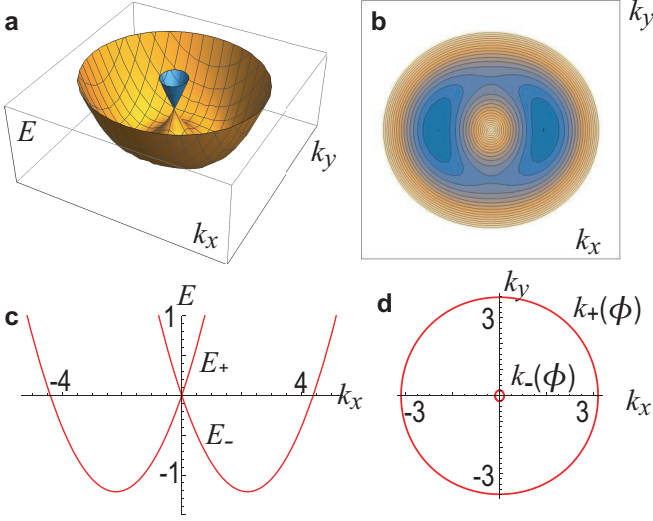


FIG. 2. **a** Bird's eye's view of the band structure. **b** Its contour plot. **c** Its cross section along the x axis. The horizontal axis is k_x in units of k_0 . **d** Fermi surfaces at $\mu = -0.2E_0$. Two circles represent Fermi surfaces $k_{\pm}(\phi)$, with $k_x = k \cos \phi$ and $k_y = k \sin \phi$. We have set $m = 4\hbar^2 k_0^2 / E_0$, $\lambda = E_0 / k_0$ and $J = 0.5E_0 / k_0$ with $E_0 \equiv m\lambda^2 / 2\hbar^2$ and $k_0 = M\lambda / 2\hbar^2$. The Néel vector is taken along the x axis, where $\Theta = \pi/2$ and $\Phi = 0$.

The band structure is shown in Fig.2, where the Néel vector is taken along the x axis. A Dirac cone exists at the momentum $k_x = k_y = 0$ as shown in Fig.2a, which is formed by the Rashba interaction. The Fermi surfaces have the p -wave symmetry as shown in Fig.2b. There are two Fermi surfaces $k_{\pm}(\phi)$ as shown in Fig.2d, where $k_x = k \cos \phi$ and $k_y = k \sin \phi$.

Drude conductivity

We first study linear conductivities. We use a perturbation theory in J assuming $|J| \ll \hbar^2 k_0 / (2M)$ with $k_0 \equiv M\lambda / 2\hbar^2$. The longitudinal Drude conductivity is calculated based on Eq.(22) in Methods, as

$$\sigma_{\text{Drude}}^{x;x} = \frac{e^2 \tau}{\hbar^2} \left[2\pi \lambda m \sqrt{\lambda^2 + \frac{2\mu}{m}} + \frac{\pi J_y (m\lambda^2 - \mu)}{\sqrt{\lambda^2 + \frac{2\mu}{m}}} \right] \quad (5)$$

for $\mu < 0$, and

$$\sigma_{\text{Drude}}^{x;x} = \frac{e^2 \tau}{\hbar^2} \pi [4\mu + 2m\lambda^2 + m\lambda J_y] \quad (6)$$

for $\mu > 0$. See the detailed derivation in Sec.II S1-1 of Supplementary Information. It is shown as a function of the chemical potential μ in Fig.3a and as a function of J_y in Fig.3b. It

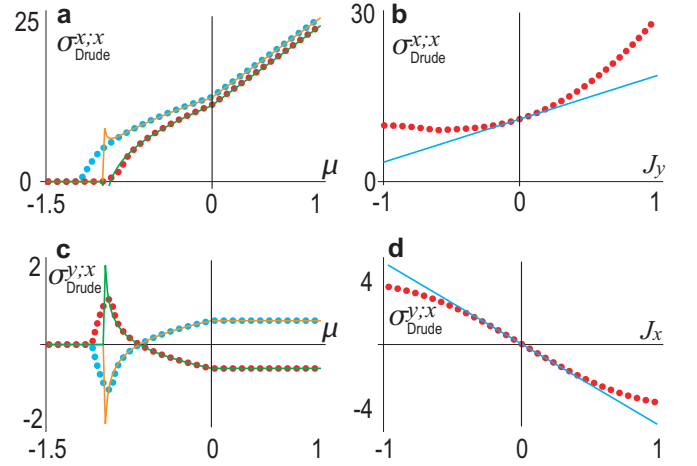


FIG. 3. **a** and **b** Longitudinal Drude conductivity $\sigma_{\text{Drude}}^{x;x}$ in the unit of $e^2 \tau / \hbar^2$, where the Néel vector is taken along the y axis. **c** and **d** Transverse Drude conductivity $\sigma_{\text{Drude}}^{y;x}$ in the unit of $e^2 \tau / \hbar^2$, where the Néel vector is taken along the x axis. **a** and **c** The horizontal axis is the chemical potential μ in units of E_0 . **b** The horizontal axis is J_y in units of E_0 . **d** The horizontal axis is J_x in units of E_0 . **a** and **c** Red (cyan) dots indicate numerically obtained results by setting $J = 0.1E_0/k_0$ ($J = -0.1E_0/k_0$). Green (orange) curves indicate analytically obtained results by setting $J = 0.1E_0/k_0$ ($J = -0.1E_0/k_0$). **b** and **d** Red dots (cyan lines) indicate numerically (analytically) obtained results by setting $\mu = -0.2E_0$. We have set $m = 4\hbar^2 k_0^2 / E_0$ and $\lambda = E_0 / k_0$.

has a dependence on the y -component J_y of the Néel vector. Hence, J_y is detectable by means of the longitudinal linear Drude conductivity.

The transverse Drude conductivity is calculated as

$$\sigma_{\text{Drude}}^{y;x} = -\frac{e^2 \tau}{\hbar^2} \pi J_x \frac{3\mu + m\lambda^2}{\sqrt{\lambda^2 + \frac{2\mu}{m}}} \quad (7)$$

for $\mu < 0$, and

$$\sigma_{\text{Drude}}^{y;x} = -\frac{e^2 \tau}{\hbar^2} m \pi \lambda J_x \quad (8)$$

for $\mu > 0$. See the detailed derivation in Sec.II S1-2 of Supplementary Information. It is proportional to the x -component J_x of the Néel vector. It is shown as a function of the chemical potential μ in Fig.3c and as a function of J_x in Fig.3d. Hence, J_x is also detectable by means of the transverse linear Drude conductivity.

We note that the sign change occurs at $\mu = -m\lambda^2/3$ in Fig.3c, which is understood analytically in Eq.(7).

Nonlinear longitudinal conductivity

We proceed to study nonlinear conductivities. In the following, we introduce magnetization, which is induced by attaching ferromagnet. We add the Hamiltonian

$$H_B = B\sigma_z, \quad (9)$$

which describes the effect of magnetization as shown in Fig.1b. Instead, this term is introduced by applying external magnetic field. The breaking of time-reversal symmetry is necessary for nonzero nonlinear conductivities[37].

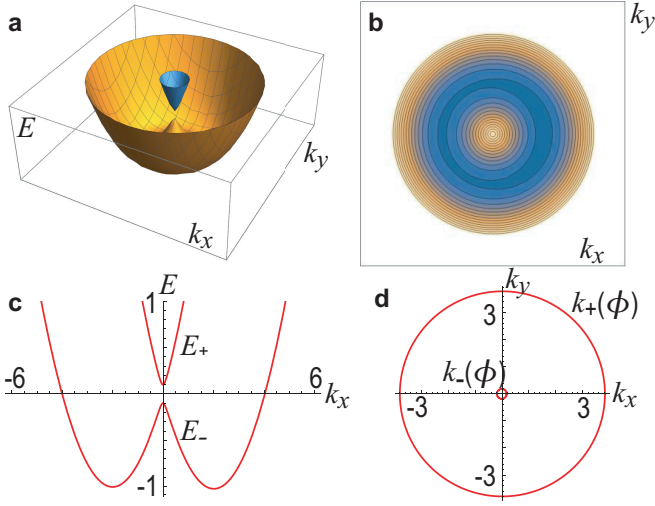


FIG. 4. **a** Bird's eye's view of the band structure. **b** Its contour plot. **c** Its cross section along the k_x axis. The horizontal axis is k_x in units of k_0 . **d** Fermi surfaces at $\mu = -0.2E_0$. We have set $m = 4\hbar^2 k_0^2/E_0$, $\lambda = E_0/k_0$, $J = 0.5E_0/k_0$ and $B = 0.1E_0$ with $E_0 \equiv m\lambda^2/2\hbar^2$ and $k_0 = M\lambda/2\hbar^2$. The Néel vector is taken along the z axis, where $\Theta = 0$ and $\Phi = 0$. Two Fermi surfaces are presented as $k_{\pm}(\phi)$, where $k_x = k \cos \phi$ and $k_y = k \sin \phi$.

The band structure is shown in Fig.4, where the Néel vector is taken along the z axis. A Dirac cone at the momentum $k_x = k_y = 0$ has a gap with $2|B|$ as shown in Fig.4a. There are two Fermi surfaces formed by the lower band E_- for $\mu < -|B|$ and formed by the lower band E_- and the upper band E_+ for $\mu > |B|$, while there is a Fermi surface formed by the lower band E_- for $|\mu| < |B|$ as shown in Fig.4c.

We first study nonlinear longitudinal conductivity. There are two contributions. One is the nonlinear Drude conductivity and the other is the quantum-metric induced nonlinear conductivity. We use a perturbation theory in J and B assuming $|J| \ll \hbar^2 k_0 / (2M)$ and $|B| \ll \hbar^2 k_0^2 / (2M)$. The nonlinear Drude conductivity at the chemical potential μ is analytically calculated based on Eq.(30) in Methods as

$$\sigma_{\text{NLDruDe}}^{xx;x} = \frac{e^3 \tau^2}{\hbar^3} \frac{3\pi \xi(\mu)}{2m\lambda \sqrt{\lambda^2 + \frac{2\mu}{m}}} B J_z, \quad (10)$$

where $\xi(\mu) = 1$ for $|\mu| > |B|$, and $\xi(\mu) = 1/2$ for $|\mu| < |B|$. It is valid for $\mu > -m\lambda^2/2$. See the detailed derivation in Sec.III S1-1 of Supplementary Information. It is proportional to the z -component J_z of the Néel vector. On the other hand, the quantum-metric induced nonlinear conductivity is analytically obtained based on Eq.(25) in Methods as

$$\sigma_{\text{Metric}}^{xx;x} = \frac{e^3}{\hbar} \frac{5\pi(\mu - m\lambda^2)}{8\mu^2 m^2 \lambda^3 \sqrt{\lambda^2 + \frac{2\mu}{m}}} B J_z \quad (11)$$

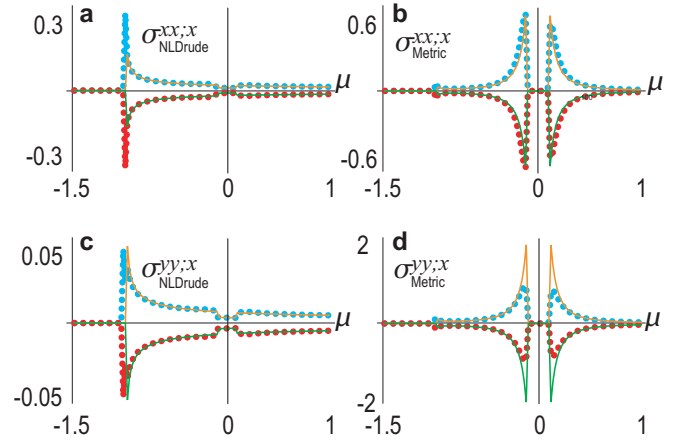


FIG. 5. μ dependence of nonlinear conductivities. **a** Nonlinear longitudinal Drude conductivity $\sigma_{\text{Drude}}^{xx;x}$ in units of $e^3 \tau^2 E_0 / (\hbar^3 k_0)$. **b** Nonlinear transverse Drude conductivity $\sigma_{\text{NLDruDe}}^{yy;x}$ in units of $e^3 \tau^2 E_0 / (\hbar^3 k_0)$. **c** Quantum-metric induced longitudinal conductivity $\sigma_{\text{Metric}}^{xx;x}$ in units of $e^3 / (\hbar E_0 k_0)$. **d** Quantum-metric induced transverse conductivity $\sigma_{\text{Metric}}^{yy;x}$ in units of $e^3 / (\hbar E_0 k_0)$. The horizontal axis is the chemical potential μ in units of E_0 . Colored dots and curves are explained in the caption of Fig.3. We have set $m = 4\hbar^2 k_0^2/E_0$, $\lambda = E_0/k_0$, $J = -0.1E_0/k_0$ and $B = 0.1E_0$. The Néel vector is taken along the z axis.

for $|\mu| > |B|$, and

$$\sigma_{\text{Metric}}^{xx;x} = \frac{e^3}{\hbar} \frac{5\pi \left(m\lambda \left(\sqrt{\lambda^2 + \frac{2\mu}{m}} + \lambda \right) - 2\mu \right)}{8m^3 \lambda^3 (m\lambda^2 - 2\mu) \left(\sqrt{\lambda^2 + \frac{2\mu}{m}} + \lambda \right)^3} B J_z \quad (12)$$

for $|\mu| < |B|$. See the detailed derivation in Sec.III S1-2 of Supplementary Information. It is also proportional to J_z . Hence, J_z is observable. The leading order of the nonlinear conductivity is proportional to $B J_z$, which means that magnetization B is necessary to detect the z -component of the Néel vector.

We show analytical results based on the perturbation theory and numerical results without using the perturbation theory. The nonlinear conductivity is shown as a function of the chemical potential μ in Fig.5. They agree with each other very well, which assures the validity of the perturbation theory. The nonlinear Drude conductivity diverges at the band bottom $\mu = -m\lambda^2/2$ and its value becomes half inside of the bulk gap $|\mu| < |B|$ comparing with the outside of the bulk gap $|\mu| > |B|$. On the other hand, the quantum-metric induced nonlinear conductivity diverges at the band edge $|\mu| = |B|$ and takes tiny value inside of the band gap $|\mu| < |B|$. Therefore, two contributions are differentiated although the explicit value of τ is unknown.

The nonlinear conductivities are shown as a function of B in Fig.6. They show nonmonotonic behavior and there is a sudden jump at $|B| = |\mu|$. It is because nonlinear conductivities depend on whether the chemical potential μ is outside of the band gap $|B|$ or inside of the band gap.

Nonlinear transverse conductivity

Next, we study nonlinear transverse conductivity. There are three contributions. Nonlinear Drude conductivity, the quantum-metric induced nonlinear conductivity and the Berry-curvature-dipole induced nonlinear conductivity. Explicit calculation shows that the Berry-curvature-dipole induced nonlinear conductivity is zero.

The nonlinear Drude conductivity at the chemical potential μ is analytically calculated based on Eq.(30) in Methods as

$$\sigma_{\text{NLDrude}}^{yy;x} = \frac{e^3 \tau^2}{\hbar^3} \frac{\pi}{2m\lambda \sqrt{\lambda^2 + \frac{2\mu}{m}}} B J_z \xi(\mu). \quad (13)$$

See the detailed derivation in Sec.III S2-1 of Supplementary Information. On the other hand, quantum-metric induced nonlinear conductivity is analytically obtained based on Eq.(25) as

$$\sigma_{\text{Metric}}^{yy;x} = \frac{e^3}{\hbar} \frac{29\pi (m\lambda^2 + \mu)}{8\mu^2 m^2 \lambda^3 \sqrt{\lambda^2 + \frac{2\mu}{m}}} B J_z \quad (14)$$

for $|\mu| > |B|$, and

$$\sigma_{\text{Metric}}^{yy;x} = \frac{e^3}{\hbar} \frac{29\pi \left(m\lambda \left(\sqrt{\lambda^2 + \frac{2\mu}{m}} + \lambda \right) - 2\mu \right)}{16m^3 \lambda^3 (m\lambda^2 - 2\mu) \left(\sqrt{\lambda^2 + \frac{2\mu}{m}} + \lambda \right)^3} B J_z. \quad (15)$$

for $|\mu| < |B|$. See the detailed derivation in Sec.III S2-2 of Supplementary Information. Hence, we can also observe J_z by measuring the nonlinear transverse conductivity. The behavior of the nonlinear transverse conductivity as a function of μ is similar to that of the nonlinear longitudinal conductivity.

Discussion

p -wave magnets have zero-net magnetization, which may lead to a high-density and ultra-fast memory as in the case of antiferromagnets and altermagnets. We have found that the Néel vector of the in-plane component of the p -wave magnet is detectable by the linear Drude conductivity without using magnetization. It is contrasted to the d -wave altermagnet, where the Néel vector is not detectable by the linear Drude conductivity but the measurement of the nonlinear conductivity is necessary[46]. On the other hand, the z -component of the Néel vector is detectable by measuring the nonlinear conductivity with the aid of magnetization.

Our results will pave a way to spintronic memory based on p -wave magnets. For example, the p -wave magnet may have easy-axis anisotropy along the x axis if we make a one-dimensional sample along the x axis. Then, the Néel vector points along the x axis, which acts as an Ising variable and can be used for a binary memory. It is detectable by measuring the linear Drude conductivity.

Methods

The energy spectrum of the Hamiltonian (1) is given by

$$E = \frac{\hbar^2 k^2}{2m} \pm \sqrt{h_x^2 + h_y^2 + h_z^2}, \quad (16)$$

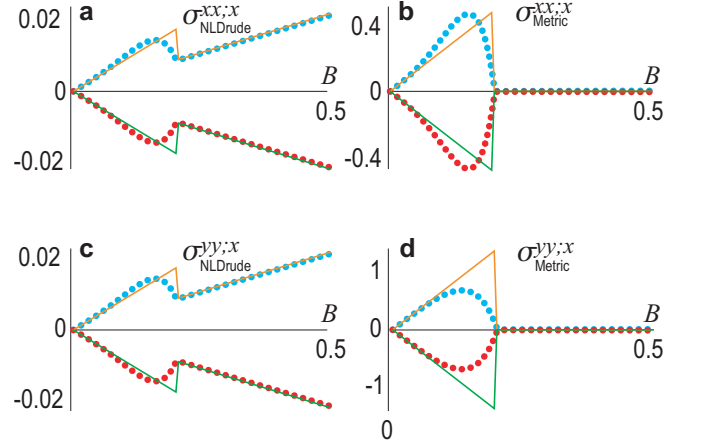


FIG. 6. B dependence of nonlinear conductivities. **a** Nonlinear longitudinal Drude conductivity $\sigma_{\text{NLDrude}}^{xx;x}$ in units of $e^3 \tau^2 E_0 / (\hbar^3 k_0)$. **b** Quantum-metric induced nonlinear longitudinal conductivity $\sigma_{\text{Metric}}^{xx;x}$ in units of $e^3 / (\hbar E_0 k_0)$. **c** Nonlinear transverse Drude conductivity $\sigma_{\text{NLDrude}}^{yy;x}$ in units of $e^3 \tau^2 E_0 / (\hbar^3 k_0)$. **d** Quantum-metric induced nonlinear transverse conductivity $\sigma_{\text{Metric}}^{yy;x}$ in units of $e^3 / (\hbar E_0 k_0)$. The horizontal axis is the magnetization B in units of E_0 . Colored dots and curves are explained in the caption of Fig.3. We have set $m = 4\hbar^2 k_0^2 / E_0$, $\lambda = E_0 / k_0$, $J = -0.1 E_0 / k_0$ and $\mu = -0.2 E_0$. The Néel vector is taken along the z axis.

where

$$h_x = -\lambda k_y + J x \sin \Theta \cos \Phi, \quad (17)$$

$$h_y = \lambda k_x + J x \sin \Theta \sin \Phi, \quad (18)$$

$$h_z = B + J x \cos \Theta. \quad (19)$$

We introduce the polar coordinate $k_x = k \cos \phi$ and $k_y = k \sin \phi$. In the first order of J and B , the energy is expanded as

$$E_{\pm} = \frac{\hbar^2 k^2}{2m} \pm \left(\frac{BJ}{\lambda} \cos \Theta \cos \phi + k\lambda - Jk \cos \phi \sin \Theta \sin(\phi - \Phi) \right). \quad (20)$$

The Fermi surfaces for the lower band E_- are obtained as

$$k_{\pm}(\phi) = m\lambda \pm mJ \cos \phi \sin \Theta \sin(\phi - \Phi) + \left(\frac{2(\mu\lambda + BJ \cos \Theta \cos \phi)}{m\lambda} + (\lambda - J \cos \phi \sin \Theta \sin(\phi - \Phi))^2 \right)^{1/2}. \quad (21)$$

The Drude conductivity is given by the formula[42]

$$\sigma^{a;b} = \frac{e^2 \tau}{\hbar^2} \sum_n \int d^2 k f_n \frac{\partial^2 E_n}{\partial k_a \partial k_b}, \quad (22)$$

where $f_n = 1 / (\exp(E_n - \mu) + 1)$ is the Fermi distribution function for the band n , and μ is the chemical potential.

The second-order nonlinear conductivity $\sigma^{ab;c}$ is expanded in terms of the electron relaxation time τ as[37]

$$\sigma^{ab;c} = \sigma_{\text{Metric}}^{ab;c} + \sigma_{\text{Dipole}}^{ab;c} + \sigma_{\text{NLDrude}}^{ab;c}, \quad (23)$$

where

$$\sigma_{\text{Metric}}^{ab;c} \propto \tau^0, \quad \sigma_{\text{Dipole}}^{ab;c} \propto \tau, \quad \sigma_{\text{NLDrude}}^{ab;c} \propto \tau^2. \quad (24)$$

First, only the term $\sigma_{\text{Metric}}^{ab;c}$ survives in the dirty limit $\tau \rightarrow 0$, which is the intrinsic nonlinear conductivity. It is the quantum-metric induced nonlinear conductivity given by[37]

$$\begin{aligned} \sigma_{\text{Metric}}^{ab;c}(\mu) &= -\frac{e^3}{\hbar} \sum_n \int d^2k f_n \left(2 \frac{\partial G_n^{ab}}{\partial k_c} - \frac{1}{2} \left(\frac{\partial G_n^{bc}}{\partial k_a} + \frac{\partial G_n^{ac}}{\partial k_b} \right) \right), \end{aligned} \quad (25)$$

where G_n^{ab} is the band–energy normalized quantum metric or the Berry connection polarizability. It is given as[27, 29, 32, 36, 37, 43]

$$G_n^{ab} = 2\text{Re} \sum_{m \neq n} \frac{A_{nm}^a(\mathbf{k}) A_{mn}^b(\mathbf{k})}{\varepsilon_n(\mathbf{k}) - \varepsilon_m(\mathbf{k})}, \quad (26)$$

with ε_n being the energy of the band n , and A_{nm}^a being the

interband Berry connection

$$A_{nm}^a(\mathbf{k}) = i \langle \psi_n(\mathbf{k}) | \partial_{k_a} | \psi_m(\mathbf{k}) \rangle. \quad (27)$$

Second, $\sigma_{\text{Dipole}}^{ab;c}$ is the nonlinear transverse conductivity induced by the Berry curvature dipole[28],

$$\sigma_{\text{Dipole}}^{ab;c}(\mu) = -\frac{e^3 \tau}{\hbar^2} \sum_n \int d^2k f_n \left(\frac{\partial \Omega_n^{bc}}{\partial k_a} + \frac{\partial \Omega_n^{ac}}{\partial k_b} \right) \quad (28)$$

with the Berry curvature

$$\Omega_n^{ab} \equiv \partial_a A_{nn}^b(\mathbf{k}) - \partial_b A_{nn}^a(\mathbf{k}). \quad (29)$$

It is an extrinsic nonlinear conductivity, since it vanishes as $\tau \rightarrow 0$.

Third, $\sigma_{\text{NLDrude}}^{ab;c}$ is the nonlinear Drude conductivity[44],

$$\sigma_{\text{NLDrude}}^{ab;c}(\mu) = -\frac{e^3 \tau^2}{\hbar^3} \sum_n \int d^2k f_n \frac{\partial^3 E_n}{\partial k_a \partial k_b \partial k_c}, \quad (30)$$

where E_n is the energy of the band n . It is also an extrinsic nonlinear conductivity.

This work is supported by CREST, JST (Grants No. JPMJCR20T2) and Grants-in-Aid for Scientific Research from MEXT KAKENHI (Grant No. 23H00171).

-
- [1] T. Jungwirth, X. Marti, P. Wadley and J. Wunderlich, Antiferromagnetic spintronics, *Nature Nanotechnology* 11, 231 (2016).
- [2] V. Baltz, A. Manchon, M. Tsoi, T. Moriyama, T. Ono, and Y. Tserkovnyak, Antiferromagnetic spintronics, *Rev. Mod. Phys.* 90, 015005 (2018).
- [3] Jiahao Han, Ran Cheng, Luqiao Liu, Hideo Ohno and Shunsuke Fukami, Coherent antiferromagnetic spintronics, *Nature Materials* 22, 684 (2023).
- [4] Zhuoliang Ni, A. V. Haglund, H. Wang, B. Xu, C. Bernhard, D. G. Mandrus, X. Qian, E. J. Mele, C. L. Kane and Liang Wu, Imaging the Neel vector switching in the monolayer antiferromagnet MnPSe₃ with strain-controlled Ising order, *Nature Nanotechnology* 16, 782 (2021).
- [5] J. Godinho, H. Reichlov, D. Kriegner, V. Novak, K. Olejnik, Z. Kašpar, Z. Šoban, P. Wadley, R. P. Campion, R. M. Otxoa, P. E. Roy, J. Železný, T. Jungwirth and J. Wunderlich, Electrically induced and detected Neel vector reversal in a collinear antiferromagnet, *Nature Communications* volume 9, Article number: 4686 (2018).
- [6] Kenta Kimura, Yutaro Otake and Tsuyoshi Kimura, Visualizing rotation and reversal of the Neel vector through antiferromagnetic trichroism, *Nature Communications*, 13, 697 (2022).
- [7] Yi-Hui Zhang, Tsao-Chi Chuang, Danru Qu, and Ssu-Yen Huang, Detection and manipulation of the antiferromagnetic Neel vector in Cr₂O₃ *Phys. Rev. B* 105, 094442 (2022).
- [8] L. Smejkal, A. H. MacDonald, J. Sinova, S. Nakatsuji and T. Jungwirth, Anomalous Hall antiferromagnets, *Nat. Rev. Mater.* 7, 482 (2022).
- [9] L. Smejkal, J. Sinova, and T. Jungwirth, Beyond Conventional Ferromagnetism and Antiferromagnetism: A Phase with Non-relativistic Spin and Crystal Rotation Symmetry, *Phys. Rev. X*, 12, 031042 (2022).
- [10] Libor Šmejkal, Jairo Sinova, and Tomas Jungwirth, Emerging Research Landscape of Altermagnetism, *Phys. Rev. X* 12, 040501 (2022).
- [11] Amar Fakhredine, Raghottam M. Sattigeri, Giuseppe Cuono, and Carmine Autieri, Interplay between altermagnetism and nonsymmorphic symmetries generating large anomalous Hall conductivity by semi-Dirac points induced anticrossings, *Phys. Rev. B* 108, 115138 (2023).
- [12] Teresa Tschirner, Philipp Keler, Ruben Dario Gonzalez Bantancourt, Tommy Kotte, Dominik Kriegner, Bernd Buechner, Joseph Dufouleur, Martin Kamp, Vedran Jovic, Libor Smejkal, Jairo Sinova, Ralph Claessen, Tomas Jungwirth, Simon Moser, Helena Reichlova, Louis Veyrat, Saturation of the anomalous Hall effect at high magnetic fields in altermagnetic RuO₂, *APL Mater.* 11, 101103 (2023)
- [13] Toshihiro Sato, Sonia Haddad, Ion Cosma Fulga, Fakher F. Assaad, Jeroen van den Brink, Altermagnetic anomalous Hall effect emerging from electronic correlations, *Phys. Rev. Lett.* 133, 086503 (2024)
- [14] Miina Leivisk Javier Rial, Anton Badura, Rafael Lopes Seeger, Ismaa Kounta, Sebastian Beckert, Dominik Kriegner, Isabelle Joumard, Eva Schmoranzero Jairo Sinova, Olena Gomonay, Andy Thomas, Sebastian T. B. Goennenwein, Helena Reichlov Libor Smejkal, Lisa Michez, Tom Jungwirth, Vincent Baltz, Anisotropy of the anomalous Hall effect in the altermagnet candidate Mn₅Si₃ films, *Phys. Rev. B* 109, 224430 (2024)
- [15] K.-H. Ahn, A. Hariki, K.-W. Lee, and J. Kunes, Antiferromagnetism in RuO₂ as d-wave Pomeranchuk instability, *Phys. Rev. B* 99, 184432 (2019).
- [16] S. Hayami, Y. Yanagi, and H. Kusunose, Momentum-

- Dependent Spin Splitting by Collinear Antiferromagnetic Ordering, *J. Phys. Soc. Jpn.* 88, 123702 (2019).
- [17] Makoto Naka, Satoru Hayami, Hiroaki Kusunose, Yuki Yanagi, Yukitoshi Motome and Hitoshi Seo, Spin current generation in organic antiferromagnets, *Nat. Com.* 10, 4305 (2019).
- [18] J. Krempask, L. Šmejkal, S. W. D'Souza, M. Hajlaoui, G. Springholz, K. Uhlov F. Alarab, P. C. Constantinou, V. Strocov, D. Usanov, W. R. Pudielko, R. Gonzez-Herndez, A. Birk Hellenes, Z. Jansa, H. Reichlov Z. Šob, R. D. Gonzalez Betancourt, P. Wadley, J. Sinova, D. Kriegner, J. Min, J. H. Dil and T. Jungwirth, Altermagnetic lifting of Kramers spin degeneracy, *Nature* 626, 517 (2024).
- [19] Suyoung Lee, Sangjae Lee, Saegyool Jung, Jiwon Jung, Donghan Kim, Yeonjae Lee, Byeongjun Seok, Jaeyoung Kim, Byeong Gyu Park, Libor Šmejkal, Chang-Jong Kang, Changyoun Kim, Broken Kramers Degeneracy in Altermagnetic MnTe, *Phys. Rev. Lett.* 132, 036702 (2024).
- [20] O. Fedchenko, J. Minar, A. Akashdeep, S.W. D'Souza, D. Vasilyev, O. Tkach, L. Odenbreit, Q.L. Nguyen, D. Kutnyakhov, N. Wind, L. Wenthau, M. Scholz, K. Rossnagel, M. Hoesch, M. Aeschlimann, B. Stadtmueller, M. Klauui, G. Schoenhense, G. Jakob, T. Jungwirth, L. Smejkal, J. Sinova, H. J. Elmers, Observation of time-reversal symmetry breaking in the band structure of altermagnetic RuO₂, *Science Advances* 10,5 (2024) DOI: 10.1126/sciadv.adj4883.
- [21] T. Osumi, S. Souma, T. Aoyama, K. Yamauchi, A. Honma, K. Nakayama, T. Takahashi, K. Ohgushi, and T. Sato, Observation of a giant band splitting in altermagnetic MnTe, *Phys. Rev. B* 109, 115102 (2024)
- [22] Zihan Lin, Dong Chen, Wenlong Lu, Xin Liang, Shiyu Feng, Kohei Yamagami, Jacek Osiecki, Mats Leandersson, Balasubramanian Thiagarajan, Junwei Liu, Claudia Felser, Junzhang Ma, Observation of Giant Spin Splitting and d-wave Spin Texture in Room Temperature Altermagnet RuO₂, arXiv:2402.04995.
- [23] Rafael Gonzalez-Hernandez, Libor Šmejkal, Karel Vborn, Yuta Yahagi, Jairo Sinova, Tomš Jungwirth, and Jakub Železn, Efficient electrical spin splitter based on nonrelativistic collinear antiferromagnetism, *Phys. Rev. Lett.*, 126:127701, (2021).
- [24] M Naka, Y Motome, and H Seo, Perovskite as a spin current generator. *Phys. Rev. B*, 103, 125114, (2021).
- [25] Arnab Bose, Nathaniel J. Schreiber, Rakshit Jain, Ding-Fu Shao, Hari P. Nair, Jiaxin Sun, Xiyue S. Zhang, David A. Muller, Evgeny Y. Tsymbal, Darrell G. Schlom & Daniel C. Ralph, Tilted spin current generated by the collinear antiferromagnet ruthenium dioxide, *Nature Electronics* 5, 267 (2022).
- [26] Anna Birk Hellenes, Tomas Jungwirth, Jairo Sinova, Libor Šmejkal, Unconventional p-wave magnets, arXiv:2309.01607.
- [27] Y. Gao, S. A. Yang, and Q. Niu, Field induced positional shift of Bloch electrons and its dynamical implications, *Phys. Rev. Lett.* 112, 166601 (2014).
- [28] I. Sodemann and L. Fu, Quantum nonlinear Hall effect induced by Berry curvature dipole in time-reversal invariant materials, *Phys. Rev. Lett.* 115, 216806 (2015).
- [29] H. Liu, J. Zhao, Y.-X. Huang, W. Wu, X.-L. Sheng, C. Xiao, and S. A. Yang, Intrinsic second-order anomalous Hall effect and its application in compensated antiferromagnets, *Phys. Rev. Lett.* 127, 277202 (2021).
- [30] Y. Michishita and N. Nagaosa, Dissipation and geometry in nonlinear quantum transports of multiband electronic systems, *Phys. Rev. B* 106, 125114 (2022).
- [31] H. Watanabe and Y. Yanase, Nonlinear electric transport in odd-parity magnetic multipole systems: Application to Mn-based compounds, *Phys. Rev. Res.* 2, 043081 (2020).
- [32] C. Wang, Y. Gao, and D. Xiao, Intrinsic nonlinear Hall effect in antiferromagnetic tetragonal cumnas, *Phys. Rev. Lett.* 127, 277201 (2021).
- [33] R. Oiwa and H. Kusunose, Systematic analysis method for nonlinear response tensors, *J. Phys. Soc. Jpn.* 91, 014701 (2022).
- [34] A. Gao, Y.-F. Liu, J.-X. Qiu, B. Ghosh, T.V. Trevisan, Y. Onishi, C. Hu, T. Qian, H.-J. Tien, S.-W. Chen et al., Quantum metric nonlinear Hall effect in a topological antiferromagnetic heterostructure, *Science* 381, eadf1506 (2023).
- [35] N. Wang, D. Kaplan, Z. Zhang, T. Holder, N. Cao, A. Wang, X. Zhou, F. Zhou, Z. Jiang, C. Zhang et al., Quantum metric-induced nonlinear transport in a topological antiferromagnet, *Nature* 621, 487 (2023).
- [36] Kamal Das, Shibalik Lahiri, Rhonald Burgos Atencia, Dimitrie Culcer, and Amit Agarwal, Intrinsic nonlinear conductivities induced by the quantum metric, *Phys. Rev. B* 108, L201405 (2023).
- [37] Daniel Kaplan, Tobias Holder and Binghai Yan, Unification of Nonlinear Anomalous Hall Effect and Nonreciprocal Magnetoresistance in Metals by the Quantum Geometry, *Phys. Rev. Lett.* 132, 026301 (2024).
- [38] YuanDong Wang, ZhiFan Zhang, Zhen-Gang Zhu, and Gang Su, Intrinsic nonlinear Ohmic current, *Phys. Rev. B* 109, 085419 (2024).
- [39] Longjun Xiang, Bin Wang, Yadong Wei, Zhenhua Qiao, and Jian Wang, Linear displacement current solely driven by the quantum metric, *Phys. Rev. B* 109, 115121 (2024).
- [40] Kazuki Maeda, Bo Lu, Keiji Yada, Yukio Tanaka, Theory of tunneling spectroscopy in p-wave altermagnet-superconductor hybrid structures, *J. Phys. Soc. Jpn.* 93, 114703 (2024).
- [41] M. Ezawa, Topological insulators based on *p*-wave altermagnets; Electrical control and detection of the altermagnetic domain wall, *Phys. Rev. B* 110, 165429 (2024).
- [42] Yuan Fang, Jennifer Cano, and Sayed Ali Akbar Ghorashi, Quantum Geometry Induced Nonlinear Transport in Altermagnets, *Phys. Rev. Lett.* 133, 106701 (2024).
- [43] Maria Teresa Mercaldo, Mario Cuoco, and Camine Ortix, Nonlinear planar magnetotransport as a probe of the quantum geometry of topological surface states, arXiv:2408.09543.
- [44] D. Kaplan, T. Holder, and B. Yan, Unifying semiclassics and quantum perturbation theory at nonlinear order, *SciPost Phys.* 14, 082 (2023).
- [45] T. Ideue, K. Hamamoto, S. Koshikawa, M. Ezawa, S. Shimizu, Y. Kaneko, Y. Tokura, N. Nagaosa, and Y. Iwasa, Bulk rectification effect in a polar semiconductor, *Nat. Phys.* 13, 578 (2017).
- [46] M. Ezawa. Detecting the Neel vector of altermagnets in heterostructures with a topological insulator and a crystalline valley-edge insulator, *Physical Review B* 109 (24), 245306 (2024).